Increased Computational Accuracy in Multi-Compartmental Cable Models by a Novel Approach for Precise Point Process Localization

A.E. LINDSAY

Department of Mathematics, University of Edinburgh, Edinburgh EH9 3JZ

K.A. LINDSAY

Department of Mathematics, University of Glasgow, Glasgow G12 8QQ

J.R. ROSENBERG*

Division of Neuroscience and Biomedical Systems, University of Glasgow, Glasgow G12 8QQ

j.rosenberg@bio.gla.ac.uk

Action Editor: Alain Destexhe

Abstract. Compartmental models of dendrites are the most widely used tool for investigating their electrical behaviour. Traditional models assign a single potential to a compartment. This potential is associated with the membrane potential at the centre of the segment represented by the compartment. All input to that segment, independent of its location on the segment, is assumed to act at the centre of the segment with the potential of the compartment. By contrast, the compartmental model introduced in this article assigns a potential to each end of a segment, and takes into account the location of input to a segment on the model solution by partitioning the effect of this input between the axial currents at the proximal and distal boundaries of segments. For a given neuron, the new and traditional approaches to compartmental modelling use the same number of locations at which the membrane potential is to be determined, and lead to ordinary differential equations that are structurally identical. However, the solution achieved by the new approach gives an order of magnitude better accuracy and precision than that achieved by the latter in the presence of point process input.

1. Introduction

Compartmental models have become important tools for investigating the behaviour of neurons to the extent that a number of packages exist to facilitate their implementation (e.g. Hines and Carnevale, 1997; Bower and Beeman, 1997). These models are constructed by replacing the continuum description of a neuron by a discrete description of the neuron formed by partitioning it into contiguous segments which interact with their nearest neighbours across common boundaries. A compartment is a mathematical representation of the morphological and biophysical properties of a segment, and a compartmental model is the collection of all compartments along with a specification of their connectivity. The efficacy of any formulation of a compartmental model depends on the faithfulness with which it captures the behaviour of the neuron that it represents, and

*To whom correspondence should be addressed.

it is in this respect that the new compartmental model developed in this article will be seen to perform better than existing compartmental models with a similar level of complexity.

The traditional approach to compartmental modelling (e.g., Rall, 1964; Segev and Burke, 1998) assigns a single potential to a compartment. This potential takes its value through an association with the average value of the current density crossing the membrane of the segment, and in a traditional compartmental model is approximated by the membrane potential at the centre of the segment. However a compartment of this type is aesthetically unsatisfactory since it cannot act as the fundamental unit in the construction of a model dendrite, first, because two compartments are required to define axial current flow, and second, because half compartments are required to represent branch points and dendritic terminals. On the other hand, the new approach to compartmental modelling assigns two potentials to a compartment—one to represent the membrane potential at the proximal boundary of the segment and the other to represent the membrane potential at its distal boundary. The new compartment can exist as an independent entity and can therefore function as the basic building block of a multi-compartmental neuronal model. Another significant difference between a traditional compartmental model and the new compartmental model lies in the novel procedure for the treatment of transmembrane current. In a traditional compartmental model the influence of transmembrane current on a segment is approximated by requiring these currents to act at the centre of the segment with the single potential assigned to the compartment representing the segment, and consequently these models do not reflect accurately the influence of the precise location of point process input[1] on the segment. By contrast, the formulation of the new compartmental model makes it more responsive to the influence of the location of point process input to a segment, and in the presence of these inputs, is shown to be an order of magnitude more accurate that a comparable traditional compartmental model.

The accuracy of the new and traditional approaches to compartmental modelling is first assessed by calculating the error in the somal potential of a test neuron when each approach is used to calculate this potential ten milliseconds after the initiation of large scale point current input. In a second comparison, the accuracy of the two approaches is assessed by comparing the statistics of the spike train output generated by each type of compartmental model of the test neuron when subjected to large scale synaptic input.

2.   Structure of Compartmental Models

We are concerned with compartmental models of dendrites. In this context, the fundamental morphological unit is the dendritic *section*, defined to be the length of dendrite connecting one branch point to a neighbouring branch point, to the soma or to a terminal. Compartmental modelling begins by subdividing each dendritic section into segments which are typically regarded as uniform circular cylinders (e.g. Segev and Burke, 1998) or tapered circular cylinders (Hines and Carnevale, 1997). In the new approach to compartmental modelling, the known membrane potentials at the ends of a segment (rather than its centre) provide the basis for the development of a set of rules which enable the influence of precisely located point process input to be partitioned between the axial current at the proximal and distal boundaries of the segment. The mathematical equations of the compartmental model are constructed by enforcing conservation of axial current at segment boundaries, dendritic branch points and dendritic terminals.

2.1.   Model Accuracy and the Partitioning of Point Process Input

The benefit in accuracy gained by taking into account the precise placement of point process input on a dendrite is best appreciated by considering how, in the absence of this facility, small variations in the location of segment boundaries exert a large influence on the solution of a traditional compartmental model. Consider, for example, a point process close to a segment boundary. A small change in the position of that boundary may move the assigned location of this point process from the centre of one segment to that of an adjacent segment. With respect to a traditional compartmental model, the location of this point process is therefore determined only to an accuracy of half a segment length, and this indeterminacy will in turn generate a model solution that is particularly sensitive to segment boundaries. Of course, with a small number of point process input, this problem can be avoided in the traditional approach to compartmental modelling by arranging that only one point process falls on a segment, and that the location of this input coincides with the centre of the

135 segment. However, this strategy is not feasible when
136 dealing with large scale point process input. What is
137 required is a procedure which describes the effect of
138 point process input on a dendritic section in a way that
139 is largely insensitive to how that section is represented
140 by segments.

141 The primary sources of error in the construction of
142 a compartmental model are the well-documented ef-
143 fect of discretising a continuous dendrite, and the less
144 well-documented error introduced by the placement of
145 point process input on the dendrite. In the traditional
146 approach based on a compartmental model with n com-
147 partments, the first type of error is $O(1/n^2)$ (by analogy
148 with the finite difference representation of derivatives),
149 but it is not widely recognised that the second type of
150 error is $O(1/n)$ whenever the input does not naturally
151 fall at the centre of segments. Since the accuracy of
152 any model is governed by the least accurate contribu-
153 tion to the model, it is clear that *in practice* the tra-
154 ditional approach to compartmental modelling in the
155 presence of point current and synaptic input is $O(1/n)$
156 accurate. This theoretical observation is supported by
157 the simulation studies of Sections 5.2 and 5.3, and by
158 an example provided for us by an anonymous reviewer.
159 This reviewer used the simulator NEURON to calculate
160 the somal potential of the test neuron shown in Fig. 3
161 10 msec after the initiation of point current. The
162 results of this calculation are shown in Table 1.

163 The results shown in the middle panel of Table 1
164 (traditional compartmental model) are based on plac-
165 ing the exogenous point current input at the centre of

166 its nearest segment, whereas the results shown in the
167 right hand panel (modified compartmental model) are
168 based on the division of the point current input be-
169 tween the centres of adjacent compartments in propor-
170 tion to the conductance between the location of the
171 input and these centres. Several important differences
172 between the two procedures for allocating the loca-
173 tion of point current input are evident from the results
174 set out in Table 1. The results based on dividing the
175 current proportionately between the centres of neigh-
176 bouring compartments converge smoothly and more
177 rapidly to the true potential than those based on the
178 traditional approach in which the current is placed at
179 the centre of the compartment. An extrapolation proce-
180 dure demonstrates that the potentials generated by the
181 modified approach converge quadratically to the true
182 somal potential as the number of compartments is in-
183 creased. Moreover, not only does the solution following
184 the traditional approach (middle panel) converge to the
185 true potential more slowly than the modified approach
186 (right hand panel), the former appears to oscillate as it
187 approaches this potential. Finally, further evidence for
188 the superior convergence of the modified approach is
189 clear from the observation that the best estimate of the
190 true potential using the traditional approach with 256
191 segments per branch section is achieved in the modified
192 approach with approximately 28 segments per branch
193 section. It will be seen in Section 4.1 that the procedure
194 used by the reviewer to partition point current input is
195 a special case of the general procedure for partitioning
point process input. By contrast with the traditional

Table 1. The somal potential of the test neuron shown in Fig. 3 is given 10 msec after the initiation of point current input. The calculation is done for nine different levels of discretisation and two methods for the placement of exogenous point current input.

Segments per branch *section*	Point current input at centre of nearest segment		Point current input divided proportionately	
	V (mV)	ΔV (mV)	V (mV)	ΔV (mV)
1	10.2355		10.5692	
2	10.2311	(-4.4616×10^{-3})	10.3357	(-2.3352×10^{-1})
4	10.2367	(5.6256×10^{-3})	10.2725	(-6.3143×10^{-2})
8	10.2333	(-3.4428×10^{-3})	10.2556	(-1.6908×10^{-2})
16	10.2470	(1.3754×10^{-2})	10.2519	(-3.6550×10^{-3})
32	10.2509	(3.8793×10^{-3})	10.2508	(-1.1320×10^{-3})
64	10.2521	(1.1874×10^{-3})	10.2506	(-2.4666×10^{-4})
128	10.2530	(8.8765×10^{-4})	10.2505	(-6.3146×10^{-5})
256	10.2511	(-1.9053×10^{-3})	10.2505	(-1.5181×10^{-5})

24   *Lindsay, Lindsay and Rosenberg*

196 approach, the new approach to compartmental mod-
197 elling describes the influence of point process input to
198 an accuracy of $O(1/n^2)$, and therefore one would an-
199 ticipate that it does not degrade the overall accuracy
200 of the model. The validity of this assertion is demon-
201 strated through the simulation studies in Sections 5.2
202 and 5.3.

203 **3. Distributed and Point Process Input**
204   **to a Segment**

205 In general, segments receive distributed and point pro-
206 cess sources of input each of which require a differ-
207 ent mathematical treatment. The current supplied by
208 distributed input such as intrinsic voltage-dependent
209 current or capacitative current is proportional to the
210 surface area of the segment on which it acts, whereas
211 the current supplied to a segment at a synapse or by an
212 exogenous point input is independent of the size of the
213 segment. An implicit assumption of a compartmental
214 model is that distributed current input to a segment is
215 small by comparison with axial current flowing along
216 the segment.
217   To appreciate why this assumption is reasonable,
218 consider a cylindrical dendritic segment of radius r
219 (cm), length h (cm) and with membrane of constant
220 conductance g_M (mS/cm^2). Suppose that axoplasm has
221 constant conductance g_A (mS/cm) and that a poten-
222 tial difference V (mV) exists between the segment
223 boundaries, then the axial current along the segment
224 is $I_A = \pi r^2 g_A V/h$ (μA) and the total distributed cur-
225 rent crossing the membrane of the segment is $I_M = $
226 $2\pi r h g_M (V/2)$. The ratio of the distributed current to
227 the axial current is therefore

$$\frac{\text{Distributed current}}{\text{Axial current}} = \frac{I_M}{I_A} = \frac{\pi r h g_M V}{\pi r^2 g_A (V/h)}$$
$$= \frac{h^2 g_M}{r g_A} = \left(\frac{h}{r}\right)^2 \frac{r g_M}{g_A}. \quad (1)$$

228 For a typical dendritic segment $r g_M/g_A$ is small (say
229 $\approx 10^{-5}$), and therefore distributed current acting on a
230 segment is small by comparison with axial current for
231 "short" segments. On the other hand, segments several
232 orders of magnitude longer than their radius can be ex-
233 pected to have distributed and axial currents of similar
234 magnitude. An important property of a compartmen-
235 tal model is that segments are not excessively long by
236 comparison with their radius (However, see Segev and
237 Burke, 1998, Fig. 3b). In the treatment of distributed

238 current, the development of the new compartmental
239 model makes explicit use of the assumption that dis-
240 tributed current is much smaller than axial current. This
241 assumption may not be valid for point process input,
242 and will not be made for the treatment of this type of
243 input in the new approach to compartmental modelling.

244 *3.1. Axial Current in the Absence*
245   *of Transmembrane Current*

246 The importance of the conclusion from Section 3 is that
247 distributed transmembrane current acting on short seg-
248 ments is small compared with axial current, and may be
249 neglected in a first approximation of the distribution of
250 membrane potential on a segment. Thus in the absence
251 of point process input, the axial current in a segment is
252 well approximated from the potential drop across the
253 segment. In the light of this approximation, consider
254 Fig. 1 which illustrates a dendritic segment of length h
255 in which $\lambda \in [0, 1]$ is the fractional distance of a point
256 of the segment from its proximal end ($\lambda = 0$). Let r_P
257 and r_D be the radii of the segment at its proximal and
258 distal boundaries respectively, let $V_P(t)$ and $V_D(t)$ be
259 the membrane potentials at these boundaries and let
260 I_{PD} be the axial current in the segment in the absence
261 of transmembrane current.
262   The membrane of the segment in Fig. 1 is formed
263 by rotating the straight line PD about the axis of the
264 dendrite to form the frustum of a cone of radius

$$r(\lambda) = (1 - \lambda)r_P + \lambda r_D, \quad \lambda \in [0, 1]. \quad (2)$$

265 Assuming that the segment is filled with axoplasm of
266 constant conductance g_A and that no current crosses
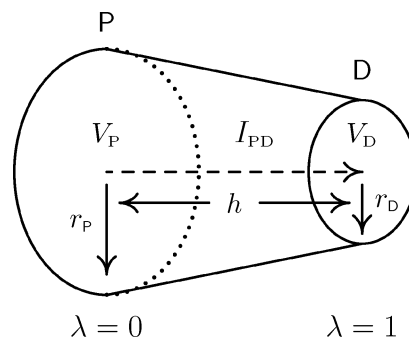

Figure 1. A segment of length h is illustrated. In the absence of transmembrane current, membrane potentials V_P and V_D at the proximal and distal boundaries of the segment generate axial current I_{PD}.

267 its membrane, then the relationship between V_P,
268 V_D and I_{PD} can be constructed by integrating the
269 defining equation of axial current, namely $I_{PD} =$
270 $-g_A A(x) dV/dx$, from the proximal to the distal
271 boundary of a segment. For the conical segment illus-
272 trated in Fig. 1, $A(x) = \pi r^2(\lambda), dV/dx = h^{-1} dV/d\lambda$
273 and the equation to be integrated is

$$I_{PD} = -\frac{g_A \pi}{h}[(1-\lambda)r_P + \lambda r_D]^2 \frac{dV}{d\lambda}$$

274 with boundary conditions $V(0) = V_P$ and $V(1) = V_D$.
275 The result of this calculation is that the the axial current
276 I_{PD} and the potentials V_P and V_D are connected by the
277 formula

$$I_{PD} = \frac{\pi g_A r_P r_D}{h}(V_P - V_D) \qquad (3)$$

278 in the absence of transmembrane current. Moreover,
279 the potential at the point λ is

$$V(\lambda) = \frac{V_P(1-\lambda)r_P + V_D \lambda r_D}{(1-\lambda)r_P + \lambda r_D}. \qquad (4)$$

280 Note that Eq. (4) is valid for sections with taper and in
281 the absence of taper will lead to a membrane potential
282 which varies linearly along the length of a segment.
283 The subsequent development of the new compartmen-
284 tal model assumes that sections may taper unless stated
285 specifically that the section is uniform.

286 *3.2. Partitioning Rule for Transmembrane Current*

287 In compartmental modelling the effect of transmem-
288 brane current is represented in the model by input
289 at points, or nodes, at which the membrane potential
290 is known. In a traditional approach to compartmental
291 modelling, these nodes are at the centre of segments,
292 whereas in the new approach they are located at the
293 boundaries of segments. The new approach partitions
294 the effect of input at any location between the nodes
295 at the proximal and distal boundaries of the segment.
296 This procedure ensures that the solution of the com-
297 partmental model is insensitive to small changes in
298 the location of segment boundaries because changes
299 in these boundaries also affect how the input is parti-
300 tioned between nodes. In the mathematical description
301 of the new compartmental model, the effect of input to
302 a segment is treated as perturbations I_P and I_D to the
303 axial current I_{PD} at the proximal and distal boundaries
304 of a segment. Axial current $I_{PD} + I_P$ is assumed to

305 leave the proximal boundary of a segment in the direc-
306 tion of its distal boundary, while axial current $I_{PD} + I_D$
307 is assumed to arrive at the distal boundary of a segment
308 from the direction of its proximal boundary. The per-
309 turbations I_P and I_D must satisfy the conservation of
310 current condition

$$(I_{PD} + I_D) - (I_{PD} + I_P) + h \int_0^1 J(\lambda, t)\, d\lambda$$

$$= 0 \rightarrow I_P - I_D = h \int_0^1 J(\lambda, t) d\lambda \qquad (5)$$

311 where $J(\lambda, t)$ denotes transmembrane current. The task
312 is to construct expressions for I_P and I_D that satisfy
313 (5) for all constitutive forms for the current density
314 $J(\lambda, t)$. The new approach to compartmental modelling
315 requires a procedure or rule for partitioning transmem-
316 brane current between the proximal and distal bound-
317 aries of a segment. The rule used in this article is that
318 transmembrane current flow to a boundary of a segment
319 is proportional to the axial conductance of the segment
320 lying between the point of application of the current
321 and that boundary. If $G_P(\lambda)$ is the axial conductance
322 of the portion of segment lying between the point λ
323 and the proximal boundary of the segment, and $G_D(\lambda)$
324 is the axial conductance of the portion of segment ly-
325 ing between the point λ and the distal boundary of the
326 segment, then

$$G_P(\lambda) = \frac{\pi g_A r_P r(\lambda)}{\lambda h}, \quad G_D(\lambda) = \frac{\pi g_A r_D r(\lambda)}{(1-\lambda)h} \quad (6)$$

327 and the rule for partitioning transmembrane current
328 leads to the expressions

$$I_P = h \int_0^1 \frac{G_P J(\lambda, t)\, d\lambda}{G_P + G_D}$$

$$= h \int_0^1 \frac{(1-\lambda)r_P\, J(\lambda, t)\, d\lambda}{(1-\lambda)r_P + \lambda r_D},$$

$$-I_D = h \int_0^1 \frac{G_D J(\lambda, t)\, d\lambda}{G_P + G_D}$$

$$= h \int_0^1 \frac{\lambda r_D\, J(\lambda, t)\, d\lambda}{(1-\lambda)r_P + \lambda r_D}. \qquad (7)$$

329 Clearly these expressions satisfy identically condition
330 (5) for the conservation of current.

26   *Lindsay, Lindsay and Rosenberg*

331 *3.3. Specification of Transmembrane Current*

332 Transmembrane current is usually assumed to consist
333 of four distinct components: capacitative current, in-
334 trinsic voltage-dependent current and point process in-
335 put which is subdivided into synaptic current and ex-
336 ogenous point current. Total transmembrane current is
337 represented by

$$\int 2\pi r \, c_M \frac{\partial V}{\partial t} \, dx + \int 2\pi r \, J_{IVDC}(V) \, dx$$
$$+ \sum J_{SYN}(V_{syn}) + \sum I_{EX} \qquad (8)$$

338 where the integrals and summations are taken over the
339 length of a segment. In this expression c_M (μF/cm^2)
340 is the specific capacitance of the segment membrane,
341 $V(x, t)$ is the distribution of membrane potential at time
342 t (msec), $J_{IVDC}(V)$ (μA/cm^2) is the density of trans-
343 membrane current due to intrinsic voltage-dependent
344 channel activity, $J_{SYN}(V_{syn})$ (μA) describes synaptic
345 input and I_{EX} (μA) describes exogenous input. Al-
346 though the specific capacitance of dendritic membrane
347 is normally taken to be constant in neuronal modelling,
348 it will be treated here as a function of position to show
349 how transmembrane current of this type may be in-
350 corporated into the new compartmental model. For a
351 segment of length h, the expression for $J(\lambda, t)$ corre-
352 sponding to formula (8) is

$$hJ(\lambda, t) = 2\pi hr(\lambda)c_M(\lambda)\frac{\partial V(\lambda, t)}{\partial t}$$
$$+ 2\pi hr(\lambda)J_{IVDC}(V(\lambda, t))$$
$$+ \sum_k J_{SYN}(V_{syn})\delta(\lambda - \lambda_k)$$
$$+ \sum_k I_{EX}(t)\delta(\lambda - \lambda_k) \qquad (9)$$

353 where λ_k denotes the relative location of the kth
354 synapse or exogenous input with respect to the proxi-
355 mal boundary of the segment ($\lambda = 0$).

356 **4. The Partitioning of Transmembrane Current**

357 Further progress requires expressions for I_P and I_D
358 in terms of the biophysical and morphological proper-
359 ties of the segment and the membrane potentials at its
360 proximal and distal boundaries. Each component of the
361 transmembrane current (9) is examined separately.

362 *4.1. Point Processes*

363 We model synaptic current by the conventional con-
364 stitutive equation $\mathcal{I} = g(t)(V - E)$ where E is the
365 reversal potential associated with the synapse and $g(t)$
366 is the time course of the synaptic conductance. Exoge-
367 nous point current input takes the form $\mathcal{I} = \mathcal{I}(t)$ where
368 $\mathcal{I}(t)$ is a known function of t. Suppose that $\lambda_1, \ldots, \lambda_n$
369 are sites of point input $\mathcal{I}_1, \ldots, \mathcal{I}_n$ to the segment, then
370 it follows from expressions (7) that the contributions
371 made to I_P and I_D from these currents are

$$I_P = \sum_{k=1}^n \frac{r_P}{r_k}(1 - \lambda_k)\mathcal{I}_k, \quad -I_D = \sum_{k=1}^n \frac{r_D}{r_k}\lambda_k\mathcal{I}_k \quad (10)$$

372 where $r_k = (1 - \lambda_k)r_P + \lambda_k r_D$. In the special case of
373 exogenous input alone, $\mathcal{I}_k = \mathcal{I}_k(t)$ and expressions (10)
374 give the exact partitioning of this input. The procedure
375 used by the anonymous reviewer (see Section 2.1) is
376 an application of Eq. (10) to a uniform segment, that
377 is,

$$I_P = \sum_{k=1}^n (1 - \lambda_k)\mathcal{I}_k, \quad -I_D = \sum_{k=1}^n \lambda_k \, \mathcal{I}_k. \quad (11)$$

378 However, when synaptic input is present, expressions
379 (10) for I_P and I_D will contain the (unknown) mem-
380 brane potentials at the synapses, and its use will there-
381 fore require these potentials to be estimated in terms of
382 known functions and the potentials at the proximal and
383 distal boundaries of the segment.
384 One obvious way to estimate the potential at the site
385 of a synapse is to use the potential distribution (4).
386 However, the efficacy of this approximation relies on
387 the validity of the assumption that transmembrane cur-
388 rent is negligible by comparison with axial current. In
389 the presence of synaptic input, transmembrane current
390 need not be negligible by comparison with axial cur-
391 rent, and so the partitioning rule must be developed to
392 include this possibility.

393 *4.2. The Partitioning Rule in the Presence*
394   *of Synaptic Input*

395 The partitioning of point process input set out in
396 Section 4.1 is developed by noting that this rule may
397 be applied to the division of transmembrane current
398 between nearest-neighbour sites of a point input, and
399 that the proximal and distal boundaries of the segment
400 are simply special cases of these sites. This application

Increased Computational Accuracy in Multi-Compartmental Cable Models   27
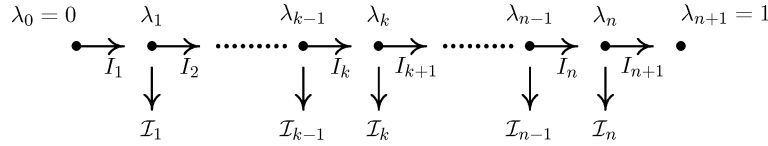

Figure 2. Configuration of point input to a dendritic segment of length h. Here $\mathcal{I}_k = g_k(t)(V_k - E_k)$ in the case of synaptic input at λ_k or $\mathcal{I}_k = \mathcal{I}_k(t)$ if the input is an exogenous point current.

401 of the partitioning rule is equivalent to considering the
402 balance between axial current and point current at each
403 site of input ignoring the influence of distributed trans-
404 membrane current between sites. The implementation
405 of the partitioning rule for general point process input
406 is done in two stages. The first stage of the discussion
407 focusses on the construction of the equations satisfied
408 by the potentials at the sites of the point input, and
409 the second stage of the discussion describes how these
410 equations may be solved numerically and is contained
411 in appendix one.

412 **4.2.1. Equations for the Potentials.** In general, the
413 locations of point process input can be taken to divide
414 a segment into sub-segments, defined to be the lengths
415 of the segment between the locations of these inputs.
416 Figure 2 is a schematic representation of a segment of
417 length h illustrating the relative locations $\lambda_1, \ldots, \lambda_n$ of
418 n point inputs $\mathcal{I}_1, \ldots, \mathcal{I}_n$ on a segment. Suppose axial
419 current I_k flows to the point λ_k from the point λ_{k-1} and
420 that V_k is the potential at the point λ_k.
421 Since distributed current alone can flow across the
422 membrane of a sub-segment, Equation (3) may be used
423 to describe the axial current in the k-th sub-segment by
424 replacing V_P and r_P with V_{k-1} and r_{k-1} respectively,
425 by replacing V_D and r_D with V_k and r_k respectively,
426 and by replacing h with $h(\lambda_k - \lambda_{k-1})$, the length of
427 the sub-segment. If $V_1, \ldots, V_n$ are the potentials at the
428 points $\lambda_1, \ldots, \lambda_n$ at which point process input is ap-
429 plied, then the axial currents $I_1, \ldots, I_{n+1}$ are related to
430 the potentials $V_1, \ldots, V_n$ by the equations

$$I_k = \frac{\pi g_A r_{k-1} r_k}{h(\lambda_k - \lambda_{k-1})}(V_{k-1} - V_k),$$
$$k = 1, \ldots, (n+1) \qquad (12)$$

431 where it is understood that $\lambda_0 = 0$, $\lambda_{n+1} = 1$, $r_0 = r_P$,
432 $r_{n+1} = r_D$, $V_0 = V_P$ and $V_{n+1} = V_D$. Equation (12)
433 are rearranged in the form

$$V_{k-1} - V_k = \frac{h}{\pi g_A} \frac{(\lambda_k - \lambda_{k-1})}{r_{k-1} r_k} I_k,$$
$$k = 1, \ldots, (n+1).$$

434 By recognising that $V_k - V_P$ is the sum of the po-
435 tential differences across the first k sub-segments,
436 it follows immediately from the previous equation
437 that

$$V_k = V_P - \frac{h}{\pi g_A} \sum_{j=1}^{k} \frac{(\lambda_j - \lambda_{j-1})}{r_{j-1} r_j} I_j,$$
$$k = 1, \ldots, n. \qquad (13)$$

438 If λ_k is the point of application of an exogenous input
439 of strength $\mathcal{I}_k(t)$ then

$$I_{k+1} + \mathcal{I}_k(t) = I_k. \qquad (14)$$

440 On the other hand, if there is a synapse at λ_k, then $\mathcal{I}_k = $
441 $g_k(t)(V_k - E_k)$ and conservation of current requires that

$$I_{k+1} + g_k(V_k - E_k) = I_k. \qquad (15)$$

442 Formula (13) for V_k is now used to rewrite Eq. (15) in
443 terms of axial currents to get

$$I_k - I_{k+1} + \frac{g_k h}{\pi g_A} \sum_{j=1}^{k} \frac{(\lambda_j - \lambda_{j-1})}{r_{j-1} r_j} I_j$$
$$= g_k(V_P - E_k), \quad k = 1, \ldots, n. \qquad (16)$$

444 Thus conservation of current at the points $\lambda_1, \cdots, \lambda_n$
445 gives rise to n equations for the $(n+1)$ currents
446 $I_1, \ldots, I_{n+1}$. In order to complete the system of equa-
447 tions specifying $I_1, \ldots, I_{n+1}$, note that the potentials at
448 the proximal and distal boundaries of the segment are
449 known, and that this condition constrains the currents
450 $I_1, \ldots, I_{n+1}$ to satisfy

$$\sum_{j=1}^{n+1} \frac{(\lambda_j - \lambda_{j-1}) r_P r_D}{r_{j-1} r_j} I_j = \frac{\pi g_A r_P r_D}{h} (V_P - V_D). (17)$$

451 Equation (17) is obtained from Eq. (13) by assert-
452 ing that $V_{n+1} = V_D$. Note also that Eq. (17) has been

28   *Lindsay, Lindsay and Rosenberg*

453 multiplied by the factor $r_P r_D$ for the benefit of numer-
454 ical work to make the coefficients of the currents in the
455 rescaled equation order one. To summarise, the cur-
456 rents $I_1, \ldots I_{n+1}$ are determined by solving the linear
457 equations

$$
\left.
\begin{aligned}
I_k - I_{k+1} &= \mathcal{I}_k(t) \\
I_k - I_{k+1} &+ \frac{g_k h}{\pi g_A} \sum_{j=1}^{k} \frac{(\lambda_j - \lambda_{j-1})}{r_{j-1} r_j} I_j \\
&= g_k(V_P - E_k),
\end{aligned}
\right\} \quad k = 1, \ldots, n
$$
$$
\sum_{j=1}^{n+1} \frac{(\lambda_j - \lambda_{j-1}) r_P r_D}{r_{j-1} r_j} I_j = \frac{\pi g_A r_P r_D}{h} (V_P - V_D)
$$
(18)

458 where the first equation is used if λ_k is the location
459 of an exogenous point input and the second equation
460 is used if λ_k is the location of a synapse. The follow-
461 ing example illustrates an application of Eq. (18) to
462 the case of a single synapse and a single exogenous
463 input.

464 *Example.*   Consider a segment which receives synap-
465 tic input of conductance $g_1(t)$ at λ_1 and exogenous cur-
466 rent $\mathcal{I}_2(t)$ at λ_2 where $0 < \lambda_1 < \lambda_2 < 1$. This parti-
467 tioning of the segment gives rise to three currents I_1,
468 I_2 and I_3. The determination of I_P and I_D will require
469 expressions for I_1 and I_3 in terms of the known con-
470 ductance $g_1(t)$, the known current $\mathcal{I}_2(t)$, the geometry
471 of the segment, and finally, the potentials V_P and V_D
472 at the proximal and distal boundaries of the segment.
473 The formulation of this problem will involve the cur-
474 rent I_2 as an auxiliary variable, but the solution for I_2
475 is not sought. It follows from Eq. (18) that I_1, I_2 and I_3
476 satisfy

$$
I_1 - I_2 + \frac{g_1(t) h}{\pi g_A} \frac{(\lambda_1 - \lambda_0)}{r_0 r_1} I_1 = g_1(t)(V_P - E_1),
$$
$$
I_2 - I_3 = \mathcal{I}_2(t), \quad (19)
$$
$$
\frac{(\lambda_1 - \lambda_0) r_0 r_3}{r_0 r_1} I_1 + \frac{(\lambda_2 - \lambda_1) r_0 r_3}{r_1 r_2} I_2 + \frac{(\lambda_3 - \lambda_2) r_0 r_3}{r_2 r_3} I_3
$$
$$
= \frac{\pi g_A r_0 r_3}{h}(V_P - V_D).
$$

477 The first Equation in (19) is Eq. (16) applied at the loca-
478 tion of the synapse ($\lambda = \lambda_1$), and the second equation
479 in (19) is Eq. (14) applied at the location of the exoge-
480 nous current ($\lambda = \lambda_2$). The last equation in (19) is

481 the consistency condition expressed by Eq. (17). Equa-
482 tions (19) can be expressed in matrix form $AX = B$
where $X = [I_1, I_2, I_3]^T$ and

483

$$
A = \begin{bmatrix}
1 + \frac{g_1(t)h}{\pi g_A} \frac{(\lambda_1 - \lambda_0)}{r_0 r_1} & -1 & 0 \\
0 & 1 & -1 \\
\frac{(\lambda_1 - \lambda_0) r_3}{r_1} & \frac{(\lambda_2 - \lambda_1) r_0 r_3}{r_1 r_2} & \frac{(\lambda_3 - \lambda_2) r_0}{r_2}
\end{bmatrix},
$$
$$
B = \begin{bmatrix}
g_1(t)(V_P - E_1) \\
\mathcal{I}_2(t) \\
\frac{\pi g_A r_0 r_3}{h}(V_P - V_D)
\end{bmatrix}.
$$

485 It is a matter of careful algebra to show that the currents
I_1 and I_3 are given by the expressions

486

$$
I_1 = \frac{\frac{\pi g_A r_0 r_3}{h}(V_P - V_D) + (1 - \lambda_1)\frac{r_0}{r_1} g_1(t)(V_P - E_1) + \mathcal{I}_2(t)(1 - \lambda_2)\frac{r_0}{r_2}}{1 + \frac{\lambda_1(1 - \lambda_1) h g_1(t)}{\pi g_A r_1^2}},
$$
$$
I_3 = \frac{\frac{\pi g_A r_0 r_3}{h}\left(1 + \frac{\lambda_1 h g_1(t)}{\pi g_A r_0 r_1}\right)(V_P - V_D) - \frac{\lambda_1 r_3}{r_1} g_1(t)(V_P - E_1)}{1 + \frac{\lambda_1(1 - \lambda_1) h g_1(t)}{\pi g_A r_1^2}} \\
\frac{- \mathcal{I}_2(t)\frac{r_3}{r_2}\left(\lambda_2 + \frac{\lambda_1(\lambda_2 - \lambda_1) h g_1(t)}{\pi g_A r_1^2}\right)}{\phantom{1 + \frac{\lambda_1(1 - \lambda_1) h g_1(t)}{\pi g_A r_1^2}}}.
$$
(20)

488 Of course, the complexity of these expressions for
489 I_1 and I_3 is in part due to the fact that they com-
490 bine the axial current in the segment in the absence
491 of point input with the modification to this current
492 due to the presence of the synaptic input at $\lambda = \lambda_1$
493 and the exogenous input at $\lambda = \lambda_2$. The perturbations
494 $I_P = I_1 - I_{PD}$ and $I_D = I_3 - I_{PD}$ to the axial cur-
495 rent at the proximal and distal boundaries of the seg-
496 ment are now calculated from formulae (3) and (20) to
497 give

498

$$
I_P = \frac{\frac{r_0(1 - \lambda_1)}{r_1} g_1(t)(\psi_1 - E_1) + \mathcal{I}_2(t)(1 - \lambda_2)\frac{r_0}{r_2}}{1 + \frac{\lambda_1(1 - \lambda_1) h g_1(t)}{\pi g_A r_1^2}},
$$
$$
- I_D
$$
$$
= \frac{\frac{\lambda_1 r_3}{r_1} g_1(t)(\psi_1 - E_1) + \mathcal{I}_2(t)\frac{r_3}{r_2}\left[\lambda_2 + \frac{g_1(t) h \lambda_1(\lambda_2 - \lambda_1)}{\pi g_A r_1^2}\right]}{1 + \frac{\lambda_1(1 - \lambda_1) h g_1(t)}{\pi g_A r_1^2}}.
$$
(21)

499   where ψ_1 is the potential

$$\psi_1 = \frac{r_0(1 - \lambda_1)V_P + r_3\lambda_1 V_D}{r_1}. \qquad (22)$$

500   It is clear from (4) that ψ_1 would be the model potential
501   at $\lambda = \lambda_1$ in the absence of transmembrane current, and
502   therefore $g_1(t)\left(\psi_1 - E_1\right)$ would be the transmembrane
503   current supplied by the synapse at $\lambda = \lambda_1$ assuming
504   that this synaptic current is negligible by comparison
505   with the axial current. Furthermore, if the common de-
506   nominator of expressions (21) is treated as unity, then
507   expressions (21) simplify to

$$I_P = \frac{r_0(1 - \lambda_1)}{r_1} g_1(t)(\psi_1 - E_1) + \mathcal{I}_2(t)(1 - \lambda_2)\frac{r_0}{r_2}, \qquad (23)$$

$$-I_D = \frac{\lambda_1 r_3}{r_1} g_1(t)(\psi_1 - E_1) + \mathcal{I}_2(t)\frac{r_3}{r_2}\lambda_2,$$

508   which are identical to Eq. (10) with $\mathcal{I}_1 = g_1(t)(\psi_1 -$
509    $E_1)$ and $\mathcal{I}_2 = \mathcal{I}(t)$. Expressions (23) are those that
510   would follow from making the assumption that trans-
511   membrane current is negligible by comparison with
512   axial current in the presence of synaptic input. Con-
513   sequently, the use of expressions (23) for I_P and I_D
514   would overestimate the true strength of both the synap-
515   tic and the exogenous input to a segment. In conclusion,
516   synaptic and exogenous input do not act independently
517   when a segment receives both types of point process
518   input.
519   The second stage of the analysis deals with the con-
520   struction and numerical solution of the equations con-
521   structed from the particular configuration of synapses
522   and exogenous input, and is given in Appendix 1.

523   *4.3.   Distributed Transmembrane Current*

524   All distributed transmembrane current is treated us-
525   ing Eq. (7) with appropriate expressions for $J(\lambda, t)$,
526   and with occurrences of the membrane potential ap-
527   proximated by expression (4). Capacitative current
528   and intrinsic voltage-dependent current are considered
529   separately.

530   **4.3.1. Capacitative Transmembrane Current.**   The
531   component of capacitative current in (9) is estimated
532   by approximating the true membrane potential along

the segment by expression (4) to obtain   533

$$J^{\text{cap}}(\lambda, t) = 2\pi c_M(\lambda) r(\lambda) \frac{dV(\lambda, t)}{dt}$$
$$= 2\pi c_M(\lambda)\left[(1 - \lambda) r_P \frac{dV_P}{dt} + \lambda r_D \frac{dV_D}{dt}\right]. \qquad (24)$$

It now follows from expressions (7) that the contribu-   534
tions made by capacitative transmembrane current to   535
I_P and to I_D are   536

$$I_P^{\text{cap}} = 2\pi\, r_P h\left[r_P \frac{dV_P}{dt}\int_0^1 \frac{(1 - \lambda)^2 c_M(\lambda)\, d\lambda}{(1 - \lambda) r_P + \lambda\, r_D}\right.$$
$$\left. + r_D \frac{dV_D}{dt}\int_0^1 \frac{\lambda(1 - \lambda)c_M(\lambda)\, d\lambda}{(1 - \lambda) r_P + \lambda\, r_D}\right], \qquad (25)$$

$$-I_D^{\text{cap}} = 2\pi\, r_D h\left[r_P \frac{dV_P}{dt}\int_0^1 \frac{\lambda(1 - \lambda)c_M(\lambda)\, d\lambda}{(1 - \lambda) r_P + \lambda\, r_D}\right.$$
$$\left. + r_D \frac{dV_D}{dt}\int_0^1 \frac{\lambda^2 c_M(\lambda)\, d\lambda}{(1 - \lambda) r_P + \lambda\, r_D}\right].$$

If the compartment is a uniform cylinder with constant   537
specific membrane capacitance, the perturbations in ax-   538
ial current at the proximal and distal boundaries of the   539
segment may be computed by evaluating the integrals   540
in formulae (25) to get   541

$$I_P^{\text{cap}} = \frac{C}{6}\left[2\frac{dV_P}{dt} + \frac{dV_D}{dt}\right],$$
$$-I_D^{\text{cap}} = \frac{C}{6}\left[\frac{dV_P}{dt} + 2\frac{dV_D}{dt}\right] \qquad (26)$$

where C is the total membrane capacitance of the seg-   542
ment. The calculation for tapered segments with non-   543
uniform membrane specific capacitance is presented in   544
Appendix 2.   545

4.3.2. Intrinsic Voltage-Dependent Transmembrane   546
Current.   The construction of I_P^{cap} and I_D^{cap} for a mem-   547
brane with non-constant specific capacitance provides   548
the framework for treating intrinsic voltage-dependent   549
transmembrane current. For an ionic species α, this   550
current is usually described by the constitutive formula   551
$J = g_\alpha(\boldsymbol{\theta})(V - E_\alpha)$ where V is the membrane poten-   552
tial, E_α is the reversal potential for species α and $g_\alpha(\boldsymbol{\theta})$ 553
is a membrane conductance which depends on a set   554
of auxiliary variables $\boldsymbol{\theta}$, for example, the probabilities   555

30   *Lindsay, Lindsay and Rosenberg*

556 m, n and h appearing in the Hodgkin-Huxley (1952)
557 model.
558   In the case of a *passive* membrane, the conductance
559 $g_\alpha(\theta)$ takes a constant (but different) value for each
560 species. The total transmembrane current density is ob-
561 tained by summing the transmembrane current densi-
562 ties of each ionic species to get

$$J = \sum_\alpha g_\alpha(V - E_\alpha) = g_M(V - E),$$

$$g_M = \sum_\alpha g_\alpha, \quad E = \sum_\alpha \frac{g_\alpha}{g_M} E_\alpha. \qquad (27)$$

563 Thus the constitutive equation for the transmembrane
564 current density of a passive membrane is $J = g_M(V -$
565 $E)$ where g_M (mS/cm^2) is the total membrane conduc-
566 tance and E plays the role of a reversal potential. When
567 the segment is a uniform cylinder with a membrane of
568 constant conductance, the contributions to I_P and I_D
569 mimic formulae (26) for capacitative current and are
570 respectively

$$I_P^{\text{IVDC}} = \frac{G}{6} [2(V_P - E) + (V_D - E)],$$

$$-I_D^{\text{IVDC}} = \frac{G}{6} [(V_P - E) + 2(V_D - E)] \qquad (28)$$

571 where G is the total membrane conductance of the
572 segment. The treatment of tapered segments with
573 non-uniform membrane conductance is presented in
574 Appendix 3.

575 **5. Comparison of the Traditional and New**
576   **Approaches to Compartmental Modelling**

577 Two simulation studies are used to compare the perfor-
578 mance of the traditional and new compartmental mod-
579 els. These studies are based on a branched model neu-
580 ron with known expression for the somal potential in re-
581 sponse to large scale exogenous input (see Appendix 4).
582 The first study examines the accuracy with which each
583 type of compartmental model estimates this somal po-
584 tential, and uses the NEURON simulator (Hines and
585 Carnevale, 1997) as an example of a traditional com-
586 partmental model. The second study assesses the ac-
587 curacy of the two types of models by comparing the
588 statistics of the spike train output generated by each
589 model when the test neuron is subjected to large scale
590 synaptic input. Here a traditional compartmental model
591 developed by the authors is used. This model gave re-
592 sults identical to those of NEURON in the first study.

593 Finally, a time step of one microsecond is used in the
594 numerical integration of each compartmental model to
595 ensure that errors in temporal integration make no sig-
596 nificant contribution to the error in the calculation of
597 membrane potential.

598 *5.1.   The Test Neuron*

599 One way to construct a branched test neuron with a
600 closed form solution for the somal potential is to choose
601 the radii and lengths of its sections such that the Rall
602 conditions for an equivalent cylinder are satisfied (Rall,
603 1964). These conditions require that the sum of the
604 three-halves power of the diameters of the child limbs
605 is equal to the three-halves power of the diameter of
606 the parent limb at any branch point, and that the total
607 electrotonic length from a branch point or the soma to
608 a dendritic tip is independent of path. The test neuron
609 illustrated in Fig. 3 satisfies these conditions. When the
610 Rall conditions are satisfied, the effect at the soma of
611 any configuration of input on the branched model of
612 the neuron is identical to the effect at the soma of the
613 unbranched equivalent cylinder with biophysical prop-
614 erties and configuration of input determined uniquely
615 from those of the original branched neuron (Lindsay
616 et al., 2003).
617   The high degree of accuracy used in the specifica-
618 tion of the dendritic radii and section lengths of the test
619 neuron is required to ensure that the equivalent cylin-
620 der is an adequate representation of the test neuron.
621 The membrane of the test neuron is assigned a specific
622 conductance of 0.091 mS/cm^2 (g_M) and specific capac-
623 itance of 1.0 μF/cm^2 (c_M), and has axoplasm of con-
624 ductance 14.286 mS/cm (g_A). With these biophysical
625 properties, the equivalent cylinder has length one elec-
626 trotonic unit. The soma of the test neuron is assumed
627 to have membrane area A_S, and specific conductance
628 g_S and specific capacitance c_S identical to that of the
629 dendritic membrane. The analytical expression for its
630 somal potential is given in Appendix 4.

631 *5.2.   First Simulation Study*

632 In this study, the performance of a traditional and
633 the new compartmental model is compared by as-
634 sessing the accuracy with which both models deter-
635 mine the time course of the somal potential of the
636 test neuron (Fig. 3) when the neuron is subjected to
637 large scale exogenous point input. Each simulation dis-

Increased Computational Accuracy in Multi-Compartmental Cable Models   31

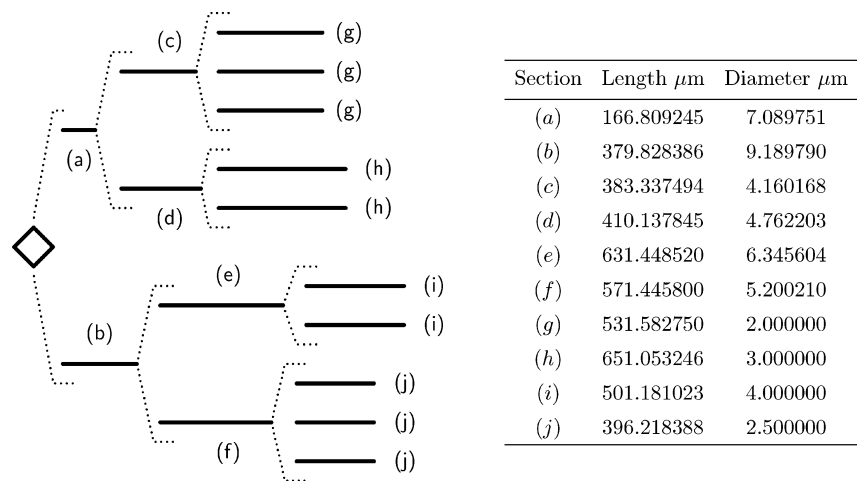| Section	Length μm	Diameter μm
(a)	166.809245	7.089751
(b)	379.828386	9.189790
(c)	383.337494	4.160168
(d)	410.137845	4.762203
(e)	631.448520	6.345604
(f)	571.445800	5.200210
(g)	531.582750	2.000000
(h)	651.053246	3.000000
(i)	501.181023	4.000000
(j)	396.218388	2.500000

Figure 3. A branched neuron satisfying the Rall conditions. The diameters and lengths of the dendritic sections are given in the right hand panel of the figure. At each branch point, the ratio of the length of a section to the square root of its radius is fixed for all children of the branch point.

tributes 75 point inputs at random over the dendritic tree of the test neuron, where each input has strength $2 \times 10^{-5}\,\mu$A. These inputs are then mapped to positions on the Rall equivalent cylinder at the same electrotonic distance from the soma (assumed to be a sphere of diameter $40\,\mu$m). The time course of the potential at the soma of the equivalent cylinder due to the combined effect of these inputs is determined analytically and taken to be the reference potential against which error in both compartmental models is measured. The difference between a computed potential and its exact value is determined at one millisecond intervals in the first 10 milliseconds of the simulation, and each difference is divided by the exact potential at that time to get a relative measure of error. The simulation procedure is repeated 2000 times to determine the statistics of the relative error for each of 13 different levels of spatial discretisation (number of compartments).

5.2.1. Results. The results for this study are set out in Table 2. This table shows the common logarithms of the mean value of the modulus of the relative error and the standard deviation of that error estimated ten milliseconds after the initiation of the stimulus. Similar results (not shown) hold for all times at which the errors were estimated.

The left hand panel of Fig. 4 shows regression lines of the common logarithms of the modulus of the mean relative error (denoted by $\overline{RE}$) for the traditional (dashed line) and new (solid line) compartmental models on the

logarithm of the number of compartments (denoted by N) used to represent the model neuron. These lines, based on the data in Table 2, have equations

$$\log_{10} \overline{RE}_{traditional} = -1.09 - 1.17 \log_{10} N,$$
$$\log_{10} \overline{RE}_{new} = -0.17 - 2.10 \log_{10} N \quad (29)$$

in which the regressions are achieved with adjusted R^2 values[2] of 97.4 and 99.5% respectively. In view of the very high R^2 values for these regression equations, a number of conclusions can be drawn from this simulation study. For a fixed number of compartments, the error in the new compartmental model is always less than that of the traditional model. The regression Eqs. (29) support the argument made in Section 2.1 that the error in a traditional compartmental model in the presence of exogenous point current input is approximately $O(1/n)$, whereas the comparable error in the new compartmental model is approximately $O(1/n^2)$. In practical terms, for example, the regression results (29) suggest that the new compartmental model with 100 compartments achieves approximately the same level of accuracy as a traditional model with 500 compartments.

The standard deviation (SD) of the modulus of the relative error can be regarded as an indicator of the reliability of a single application of the model. The right hand panel of Fig. 4 shows regression lines of the common logarithms of the standard deviation of the modulus of the relative error for the traditional (dashed line) and new (solid line) compartmental models on the logarithm of the number of compartments used to

32   *Lindsay, Lindsay and Rosenberg*

Table 2.   The result of 2000 simulations for each of 13 different levels of discretisation used in the implementation of a traditional and new compartmental model. The common logarithms of the mean value of the modulus of the relative error and the standard deviation of that error are estimated at ten milliseconds after the initiation of the stimulus.

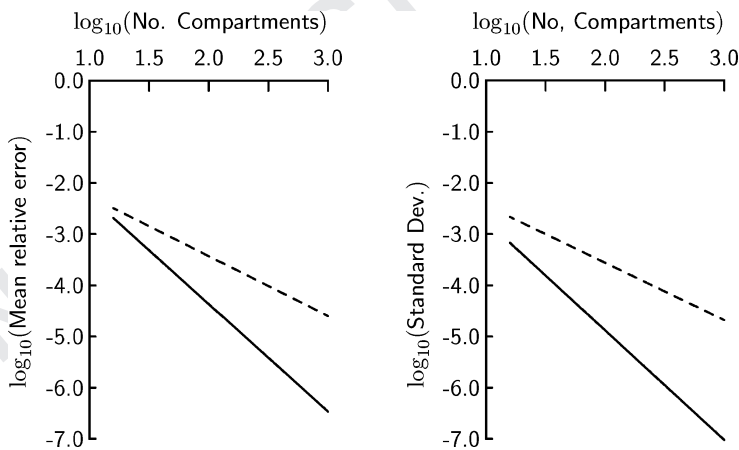| Compartments ($\log_{10}$(compartments))		Traditional new model $\log_{10}$(mean)		Traditional new model $\log_{10}$(standard dev.)	
17	(1.2305)	−2.41151	−2.71945	−2.62290	−3.19338
21	(1.3222)	−2.47233	−2.77674	−2.69851	−3.24583
34	(1.5314)	−2.94299	−3.41196	−3.06731	−3.88820
41	(1.6127)	−3.04729	−3.62138	−3.17081	−4.14997
54	(1.7323)	−3.21258	−3.89150	−3.34889	−4.41251
61	(1.7853)	−3.24692	−3.91268	−3.37653	−4.45051
75	(1.8750)	−3.35180	−4.12056	−3.46881	−4.65463
82	(1.9138)	−3.39846	−4.23567	−3.51591	−4.76498
93	(1.9684)	−3.45602	−4.30636	−3.57633	−4.82045
193	(2.2855)	−3.77417	−4.94731	−3.89829	−5.47886
293	(2.4668)	−3.94409	−5.31876	−4.07811	−5.84771
390	(2.5910)	−4.08234	−5.57349	−4.20025	−6.10791
495	(2.6946)	−4.15996	−5.78252	−4.28525	−6.32790

Figure 4.   The left panel shows the regression lines of the common logarithm of the mean relative errors in the new compartmental model (solid line) and a traditional compartmental model (dashed line) against the common logarithm of the number of compartments. All errors are measured ten milliseconds after initiation of the stimulus. The right panel shows the regression lines for the standard deviations of the mean relative errors for the new compartmental model (solid line) and for a traditional compartmental model (dashed line).

695 represent the model neuron. These lines, based on the
696 data in Table 2, have equations

$$\log_{10} \mathrm{SD}_{traditional} = -1.32 - 1.12 \log_{10} N \,,$$
$$\log_{10} \mathrm{SD}_{new} = -0.60 - 2.14 \log_{10} N \tag{30}$$

in which the regressions are achieved with adjusted R^2

values of 98.7 and 99.4% respectively. These regres- 697
sion lines show that the new compartmental model is 698
more reliable than a traditional compartmental model. 699
For example, a traditional compartmental model re- 700
quires at least 100 compartments to give a standard 701
deviation of the modulus of the relative error that is 702
smaller than that of the new compartmental model us- 703
ing 40 compartments. 704

Increased Computational Accuracy in Multi-Compartmental Cable Models   33
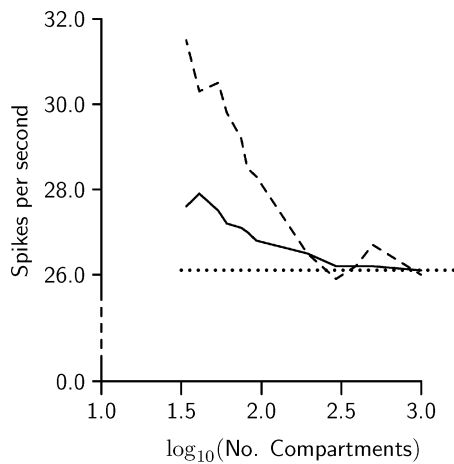

Figure 5. The spike rate plotted against the common logarithm of the number of compartments for a traditional compartmental model (dashed line) and the new compartmental model (solid line). The dotted line shows the expected spike rate.

705 5.3.   *Second Simulation Study*

706 In the second simulation study 100 synapses are dis-
707 tributed at random over the dendritic tree of the test
708 neuron illustrated in Fig. 3. Each synapse is activated
709 independently of all other synapses, has a maximum
710 conductance of 3×10^{-5} mS and a rise time of 0.5
711 msec. Activation times for each synapse follow Pois-
712 son statistics with a mean rate of 30 pre-synaptic spikes
713 per second. Spikes are generated by the soma of the test
714 neuron using Hodgkin-Huxley kinetics. This study is
715 based on 12 different levels of spatial discretisation
716 (number of compartments) in which each simulation
717 of the traditional and new compartmental models use
718 identical synaptic firing times and identical numbers of
719 compartments.

720 **5.3.1. Results.**   Table 5 gives the spike rate of soma-
721 generated action potentials based on 11 seconds of ac-
722 tivity, the first second of which is ignored.
723   Figure 5 illustrates the data set out in Table 3 in
724 which the spike rates for the traditional model (dashed
725 line) and new model (solid line) are plotted against
726 the common logarithm of N, the number of compart-
727 ments used in each simulation. As N is increased, the
728 spike rates generated by both models approach a com-
729 mon limit. However, the spike rate generated by the
730 traditional model approaches this limit more slowly
731 and appears to oscillate as the limit is approached. The
732 spike rate obtained using the traditional model with 500
733 compartments is achieved in the new model with only

Table 3.   The spike rate estimated from a 10 second record of spike train activity obtained from a traditional and the new compartmental model at 12 different levels of spatial discretisation (number of compartments).

Compartments ($\log_{10}$(Compartments))		Traditional model mean firing rate	New model mean firing rate
34	(1.5314)	31.5	27.6
41	(1.6127)	30.3	27.9
54	(1.7323)	30.5	27.5
61	(1.7853)	29.8	27.2
75	(1.8750)	29.2	27.0
82	(1.9138)	28.5	27.0
93	(1.9684)	28.3	26.8
193	(2.2855)	26.5	26.5
293	(2.4668)	25.9	26.2
390	(2.5910)	26.2	26.2
495	(2.6946)	26.7	26.2
992	(2.9965)	26.0	26.1

734 100 compartments. These differences in the number of
735 compartments required to achieve the same level of ac-
736 curacy in both models are identical to those observed
737 in the first study.

738 **5.3.2. Comparison of Model-Generated Spike Trains.**
739 It is clear from Fig. 5 that the mean rate of the spike train
740 generated by the new compartmental model converges
741 more quickly to the theoretical mean spike rate than
742 that generated by a traditional compartmental model.
743 One would therefore infer from the behaviour of this
744 summary statistic that the spike train generated by the
745 former is a more accurate representation of the spiking
746 behaviour of the test neuron in response to synaptic
747 activity than that generated by the latter. To investi-
748 gate the validity of this inference requires an accurate
749 comparison of the times of occurrence of the spikes in
750 the spike trains generated by each model with identical
751 synaptic activity applied to the test neuron. We take
752 as our reference the times of occurrence of the spikes
753 generated in ten seconds using the new compartmen-
754 tal model with 100 compartments (spike train $\mathcal{N}_{100}$).
755 These spike times are compared with those generated
756 by a traditional compartmental model with 100 com-
757 partments and with 500 compartments[3] (spike trains
758 $\mathcal{T}_{100}$ and $\mathcal{T}_{500}$ respectively). The times of occurrence of
759 spikes in the spike trains to be compared are taken to be
760 identical if they occur within one millisecond of each
761 other. The comparison between $\mathcal{N}_{100}$ and $\mathcal{T}_{100}$ revealed
762 244 spikes common to both spike trains (i.e. occurring

34   *Lindsay, Lindsay and Rosenberg*

763 within one millisecond of each other). There were 24
764 spikes unique to $\mathcal{N}_{100}$ and 39 spikes unique to $\mathcal{T}_{100}$. The
765 comparison between $\mathcal{N}_{100}$ and $\mathcal{T}_{500}$ revealed 258 spikes
766 common to both spike trains with 10 spikes unique to
767 $\mathcal{N}_{100}$ and 9 spikes unique to $\mathcal{T}_{500}$. Since the reference
768 spike train $\mathcal{N}_{100}$ is common to both comparisons, it
769 is clear that as the number of compartments in a tradi-
770 tional model increases, the spike train generated by that
771 model will conform more closely to that generated by
772 the new compartmental model with significantly fewer
773 compartments.

774 **6. Concluding Remarks**

775 We have demonstrated that it is possible to achieve
776 a significant increase in the accuracy and precision
777 of compartmental models by developing a new com-
778 partmental model in which compartments have two
779 potentials—one at either end of the segment which the
780 compartment represents. The new compartment acts
781 as fundamental unit in the construction of a model of a
782 branched dendrite. When these compartments are con-
783 nected by requiring continuity of potential and conser-
784 vation of current at segment boundaries, they provide a
785 new type of compartmental model with a mathematical
786 form identical to that of a traditional model in the sense
787 that both types of compartmental model involve only
788 nearest neighbour interactions. One demonstrated ben-
789 efit of the new compartmental model is that it provides
790 a mechanism to take account of the exact location of
791 point process input by contrast with traditional com-
792 partmental models which would assign this input to an
793 accuracy of half the length of a segment. We would an-
794 ticipate that the application of the new compartmental
795 model would be most useful in association with exper-
796 iments in which the precise timing of spikes is thought
797 to be important (e.g., Oram et al., 1999 and the refer-
798 ences therein) or in studies investigating the influence
799 of the location of synaptic input on the mean rate of the
800 spike train output (e.g., Poirazi et al., 2003).

801 **Appendix 1: Numerical Estimation of**
802 **Perturbations to Axial Current**

803 The example in Section 4.2 demonstrates that synap-
804 tic and exogenous input do not act independently. This
805 means that both types of point process input must be
806 treated simultaneously in the construction of the equa-
807 tions to determine the perturbations I_P and I_D of the

808 axial current. The equations for the perturbations in ax-
809 ial current are constructed by replacing I_k in Eqs. (14),
810 (16 and 17) by $I_{PD} + \hat{I}_k$ where $\hat{I}_k$ is the perturbation
811 to I_k. If $\lambda = \lambda_k$ is the site of an exogenous input then
812 the appropriate equation for the perturbed currents is

$$\hat{I}_k - \hat{I}_{k+1} = \mathcal{I}_k(t), \qquad (31)$$

813 whereas if $\lambda = \lambda_k$ is the site of a synapse with conduc-
814 tance $g_k(t)$, the appropriate equation is

$$\hat{I}_k - \hat{I}_{k+1} + \frac{g_k h}{\pi g_A} \sum_{j=1}^{k} \frac{(\lambda_j - \lambda_{j-1})}{r_{j-1} r_j} \hat{I}_j = \mathcal{I}_k(t) \quad (32)$$

815 where the current $\mathcal{I}_k(t)$ is defined by the formula

$$\mathcal{I}_k(t) = g_k(t)\left[(1 - \lambda_k)\frac{r_P}{r_k} V_P + \lambda_k \frac{r_D}{r_k} V_D - E_k \right]. \quad (33)$$

The derivation of Eq. (32) takes advantage of the iden-
tity

$$\sum_{j=1}^{k} \frac{(\lambda_j - \lambda_{j-1})}{r_{j-1} r_j} = \frac{\lambda_k}{r_P r_k},$$

816 which can be established by induction. Note that ex-
817 pression (33) for $\mathcal{I}_k(t)$ when $\lambda = \lambda_k$ is a synapse is
818 precisely the current that would be expected to flow at
819 the synapse if the distribution of potential on the seg-
820 ment was described by expression (4). Finally, Eq. (17)
821 simplifies to

$$\sum_{j=1}^{n+1} \frac{(\lambda_j - \lambda_{j-1})r_P r_D}{r_{j-1} r_j} \hat{I}_j = 0 \qquad (34)$$

822 where the constant multiplier $r_P r_D$ has been added
823 without loss to make the coefficients of this equation
824 comparable to those appearing in the first n equations.
825 Eqs. (31), (32) and (34) may be represented compactly
826 in matrix notation by

$$A \hat{I} + GC \hat{I} = \mathcal{I} \qquad (35)$$

827 where $\hat{I} = [\hat{I}_1, \ldots, \hat{I}_{n+1}]^T$ is the $(n + 1)$ dimensional
828 column vector of perturbations in axial current, $\mathcal{I} =$
829 $[\mathcal{I}_1, \ldots, \mathcal{I}_n, 0]^T$ and A is the $(n + 1) \times (n + 1)$ matrix

830

$$\begin{bmatrix}
1 & -1 & 0 & \cdots & \cdots & 0 \\
0 & 1 & -1 & \cdots & \cdots & 0 \\
0 & 0 & 1 & \cdots & \cdots & 0 \\
\cdots & \cdots & \cdots & \cdots & \cdots & \cdots \\
0 & 0 & 0 & \cdots & 1 & -1 \\
\dfrac{\lambda_1 r_P r_D}{r_0 r_1} & \dfrac{(\lambda_2 - \lambda_1) r_P r_D}{r_1 r_2} & \dfrac{(\lambda_3 - \lambda_2) r_P r_D}{r_2 r_3} & \cdots & \dfrac{(\lambda_n - \lambda_{n-1}) r_P r_D}{r_{n-1} r_n} & \dfrac{(1 - \lambda_n) r_P r_D}{r_n r_{n+1}}
\end{bmatrix}.$$
$$(36)$$

831 Briefly, G is an $(n + 1) \times (n + 1)$ diagonal matrix
832 in which the (k, k) entry is zero if λ_k is the site of an
833 exogenous input and takes the value $g_k(t)$ if λ_k is the
834 site of a synapse. The $(n+1, n+1)$ entry of G is always
835 zero. The matrix C is a lower triangular matrix of type
836 $(n + 1) \times (n + 1)$ in which all the nonzero entries in the
837 k^{th} column take the value $(\lambda_k - \lambda_{k-1})/(\pi g_A r_{k-1} r_k)$.

838 *Multiple Point Inputs*

839 To take account of the influence of the matrix GC in
840 the solution of Eq. (35), the algorithm

$$A \hat{I}^{(m+1)} = \mathcal{I} - GC \hat{I}^{(m)} \qquad (37)$$

841 is iterated with initial condition $A \hat{I}^{(0)} = \mathcal{I}$. Although
842 it can be demonstrated that the matrix A has a simple
843 closed form expression for its inverse, it is not (numer-
844 ically) efficient to use this expression to solve Eq. (37).
845 Instead, we observe that A has an LU factorisation
846 in which U is the $(n + 1) \times (n + 1)$ upper triangular
847 matrix with ones everywhere in the main diagonal, neg-
848 ative ones everywhere in the super-diagonal and zero
849 everywhere else, and L is the $(n + 1) \times (n + 1)$ lower
850 triangular matrix

$$\begin{bmatrix}
1 & 0 & 0 & 0 & \cdots & \cdots & 0 \\
0 & 1 & 0 & 0 & \cdots & \cdots & 0 \\
0 & 0 & 1 & 0 & \cdots & \cdots & 0 \\
\cdots & \cdots & \cdots & \cdots & \cdots & \cdots & \cdots \\
\dfrac{\lambda_1 r_P}{r_1} & \dfrac{\lambda_2 r_P}{r_2} & \dfrac{\lambda_3 r_P}{r_3} & \dfrac{\lambda_4 r_P}{r_4} & \cdots & \dfrac{\lambda_n r_P}{r_n} & 1
\end{bmatrix} (38)$$

851 Since $\mathcal{I}$ is a linear combination of V_P, V_D and a voltage
852 independent term, then the solution to Eq. (37) has
853 general representation

$$\hat{I} = \phi_1(t) V_P + \phi_2(t) V_D + \phi_3(t) \qquad (39)$$

where $\phi_1(t)$, $\phi_2(t)$ and $\phi_3(t)$ satisfy **854**

$$A \phi_1 = \left[g_1(1 - \lambda_1) \frac{r_P}{r_1}, \ldots, g_n(1 - \lambda_n) \frac{r_P}{r_n}, 0 \right]^{\mathrm{T}}$$
$$- GC \phi_1, \qquad (40)$$
$$A \phi_2 = \left[g_1 \lambda_1 \frac{r_D}{r_1}, \ldots, g_n \lambda_n \frac{r_D}{r_n}, 0 \right]^{\mathrm{T}} - GC \phi_2,$$
$$A \phi_3 = -[g_1 E_1, \ldots, g_n E_n, 0]^{\mathrm{T}} - GC \phi_3.$$

The Eqs. (40) for $\phi_1(t)$, $\phi_2(t)$ and $\phi_3(t)$ may be solved **855**
easily by an iterative procedure based on the sparse **856**
LU factorisation of A. If the conductances $g_1, \cdots, g_n$ **857**
are sufficiently small, the solution of Eqs. (40) is well **858**
approximated by ignoring the second term on the right **859**
hand side or Eqs. (40). This approximation is equivalent **860**
to using the partitioning rule (7) in combination with **861**
formula (4) for the membrane potential. **862**

Special Case of Exogenous Input **863**

If $\lambda_1, \cdots, \lambda_n$ are sites of exogenous input $\mathcal{I}_1, \cdots, \mathcal{I}_n$ **864**
then $G = 0$ in Eq. (37) and $\mathcal{I}$ is the vector of exogenous **865**
currents. In this case, expressions (10) for I_P and I_D **866**
are obtained immediately as the first and last entries in **867**
the solution $\hat{I}$ of equation $A \hat{I} = LU \hat{I} = \mathcal{I}$. **868**

Appendix 2: The Partitioning of Capacitive **869**
Current on Tapered Cylinders **870**

Recall from expressions (7) that the contributions made **871**
to the proximal and distal perturbations to the axial cur- **872**
rent as a consequence of capacitive transmembrane **873**
current on a tapered segment with membrane of vari- **874**
able specific capacitance are respectively **875**

$$I_P^{\text{cap}} = 2\pi r_P h \left[r_P \frac{dV_P}{dt} \int_0^1 \frac{(1 - \lambda)^2 c_M(\lambda) \, d\lambda}{(1 - \lambda) r_P + \lambda r_D} \right.$$
$$\left. + r_D \frac{dV_D}{dt} \int_0^1 \frac{\lambda(1 - \lambda) c_M(\lambda) \, d\lambda}{(1 - \lambda) r_P + \lambda r_D} \right],$$

$$-I_D^{\text{cap}} = 2\pi r_D h \left[r_P \frac{dV_P}{dt} \int_0^1 \frac{\lambda(1 - \lambda) c_M(\lambda) \, d\lambda}{(1 - \lambda) r_P + \lambda r_D} \right.$$
$$\left. + r_D \frac{dV_D}{dt} \int_0^1 \frac{\lambda^2 c_M(\lambda) \, d\lambda}{(1 - \lambda) r_P + \lambda r_D} \right]. \quad (41)$$

36   *Lindsay, Lindsay and Rosenberg*

876 For tapered segments ($r_P \neq r_D$) with membranes of
877 non-uniform specific capacitance, the integrals in (41)
878 have values

$$I_P^{\text{cap}} = 2\pi h \, r_P [c_P \psi(r_P, r_D) + c_D \phi(r_P, r_D)] \frac{dV_P}{dt}$$
$$+ 2\pi h [c_P r_D \phi(r_P, r_D) + c_D r_P \phi(r_D, r_P)] \frac{dV_D}{dt},$$
$$-I_D^{\text{cap}} = 2\pi h [c_P r_D \phi(r_P, r_D) + c_D r_P \phi(r_D, r_P)] \frac{dV_P}{dt}$$
$$+ 2\pi h r_D [c_P \phi(r_D, r_P) + c_D \psi(r_D, r_P)] \frac{dV_D}{dt}$$
$$(42)$$

879 where $c_M(\lambda) = (1 - \lambda)c_P + \lambda c_D$ and the auxiliary
880 functions $\phi(x, y)$ and $\psi(x, y)$ are defined by

$$\phi(x, y) = \frac{x}{6(x - y)^3}$$
$$\times \left[x^2 - 5xy - 2y^2 + \frac{6xy^2}{x - y} \log \frac{x}{y} \right],$$
$$\psi(x, y) = \frac{x}{6(x - y)^3} \qquad (43)$$
$$\times \left[2x^2 - 7xy + 11y^2 - \frac{6y^3}{x - y} \log \frac{x}{y} \right].$$

881 The evaluation of the integrals in expression (41) is
882 facilitated by defining the auxiliary integrals

$$\mathcal{K}_1 = \int_0^1 \frac{(1 - \lambda)^2 \hat{c}_M(\lambda) \, d\lambda}{\hat{r}(\lambda)},$$
$$\mathcal{K}_2 = \int_0^1 \frac{\lambda(1 - \lambda)\hat{c}_M(\lambda) \, d\lambda}{\hat{r}(\lambda)},$$
$$\mathcal{K}_3 = \int_0^1 \frac{\lambda^2 \hat{c}_M(\lambda) \, d\lambda}{\hat{r}(\lambda)}$$

883 and observing that $\mathcal{K}_1$, $\mathcal{K}_2$ and $\mathcal{K}_3$ can be determined
884 easily from the identities

$$\mathcal{K}_1 + 2\mathcal{K}_2 + \mathcal{K}_3 = \int_0^1 \frac{\hat{c}_M(\lambda) \, d\lambda}{\hat{r}(\lambda)},$$
$$r_P \mathcal{K}_1 + r_D \mathcal{K}_2 = \int_0^1 (1 - \lambda)\hat{c}_M(\lambda) \, d\lambda,$$
$$r_P \mathcal{K}_2 + r_D \mathcal{K}_3 = \int_0^1 \lambda \hat{c}_M(\lambda) \, d\lambda.$$

885 The results given in Section 4.3.1 for a uniform segment
886 ($r_P = r_D$) are obtained from formulae (42) by replac-
887 ing $\phi(x, y)$ and $\psi(x, y)$ with their respective limiting

values of 1/12 and 1/4 where each limit is taken as **888**
$x \to y$. **889**

Appendix 3: Partitioning of Voltage-Dependent **890**
Current on Tapered Cylinders **891**

The construction of I_P^{cap} and I_D^{cap} for a membrane with **892**
non-constant specific capacitance provides the frame- **893**
work for treating intrinsic voltage-dependent trans- **894**
membrane current. For tapered segments with non- **895**
constant membrane conductance, the contributions to **896**
the perturbations in the axial current at the proximal **897**
and distal boundaries of the segment are identical to **898**
expressions (42) with c_P replaced by $g_P(V_P; \boldsymbol{\theta})$ and **899**
c_D replaced by $g_D(V_D; \boldsymbol{\theta})$. These contributions are **900**

$$I_P^{\text{IVDC}} = 2\pi h \, r_P [g_P(V_P; \boldsymbol{\theta}) \, \psi(r_P, r_D)$$
$$+ g_D(V_D; \boldsymbol{\theta}) \phi(r_P, r_D)](V_P - E)$$
$$+ 2\pi h [g_P(V_P; \boldsymbol{\theta}) \, r_D \phi(r_P, r_D)$$
$$+ g_D(V_D; \boldsymbol{\theta}) \, r_P \phi(r_D, r_P)](V_D - E),$$
$$-I_D^{\text{IVDC}} = 2\pi h [g_P(V_P; \boldsymbol{\theta}) \, r_D \phi(r_P, r_D)$$
$$+ g_D(V_D; \boldsymbol{\theta}) \, r_P \phi(r_D, r_P)](V_P - E)$$
$$+ 2\pi h \, r_D [g_P(V_P; \boldsymbol{\theta}) \, \phi(r_D, r_P)$$
$$+ g_D(V_D; \boldsymbol{\theta}) \, \psi(r_D, r_P)](V_D - E) \quad (44)$$

where the auxiliary functions $\phi(x, y)$ and $\psi(x, y)$ are **901**
defined in (43). **902**

Appendix 4: Analytical Solution for Somal **903**
Potential of Test Neuron **904**

It may be shown that $V(t)$, the deviation of the somal **905**
transmembrane potential from its resting value as a **906**
result of a distribution $\mathcal{I}(x, t)$ of current on a uniform **907**
cylindrical dendrite of radius a and length l attached to **908**
a soma is **909**

$$V(t) = e^{-t/\tau} \left[\phi_0(t) + \sum_\beta \phi_\beta(t) e^{-\beta^2 t/L^2 \tau} \cos \beta \right],$$
$$L = l \sqrt{\frac{2g_M}{ag_A}} \qquad (45)$$

where τ is the time constant of the somal and dendritic **910**
membranes and g_M and g_A have their usual meanings. **911**
The summation is taken over all the solutions β of the **912**
transcendental equation $\tan \beta + \gamma \beta = 0$ where γ (con- **913**
stant) is the ratio of the total membrane area of the soma **914**

to the total membrane area of the dendrite. The functions $\phi_0(t)$ and $\phi_\beta(t)$ are solutions of the differential equations

$$\frac{d\phi_0}{dt} = -\frac{e^{t/\tau}}{C_D + C_S}\left[\mathcal{I}_S(t) + \int_0^l \mathcal{I}(x,t)\,dx\right],$$

$$\frac{d\phi_\beta}{dt} = -\frac{2e^{(1+\beta^2/L^2)t/\tau}}{C_D + C_S\cos^2\beta}\left[\int_0^1 \mathcal{I}(x,t)\cos\beta\right.$$

$$\left.\times(1-x/l)\,dx + \cos\beta\,\mathcal{I}_S(t)\right] \quad (46)$$

with initial conditions $\phi_0(0) = \phi_\beta(0) = 0$, that is, the neuron is initialised at its resting potential. The parameters C_S and C_D denote respectively the total membrane capacitances of the soma and dendrite, and $\mathcal{I}_S(t)$ is the current supplied to the soma.

In the special case in which point currents $\mathcal{I}_1(t),\ldots,\mathcal{I}_n(t)$ act at distances $x_1,\ldots x_n$ from the soma of the uniform cylinder, the corresponding coefficient functions ϕ_0 and ϕ_β satisfy

$$\frac{d\phi_0}{dt} = -\frac{e^{t/\tau}}{C_D + C_S}\left[\mathcal{I}_S(t) + \sum_{k=1}^n \mathcal{I}_k(t)\right],$$

$$\frac{d\phi_\beta}{dt} = -\frac{2e^{(1+\beta^2/L^2)t/\tau}}{C_D + C_S\cos^2\beta}$$

$$\times\left[\sum_{k=1}^n \mathcal{I}_k(t)\cos\beta(1-x_k/l) + \cos\beta\,\mathcal{I}_S(t)\right].$$

$$(47)$$

Acknowledgment

Notes

1. Following the terminology of Hines and Carnevale (Hines97, a point process is taken to mean either synaptic input (voltage-dependent) or an exogenous point current input (voltage-independent).
2. R^2 measures the proportion of the total variation of the dependent variable about its mean value that is explained by the regression, and necessarily takes a value between zero and one expressed as a percentage.
3. All the simulations were run on a PC with dual Athlon 1500MP processors. The times required to simulate 10 seconds of spike train data were 61 minutes for the new compartmental model with 100 compartments, 41 minutes and 353 minutes for a traditional compartmental model with 100 and 500 compartments respectively. In the presence of point current input alone, the computational times for both models are identical.

References

Bower JM, Beeman D (1997) The Book of GENESIS, 2nd edition. NY Telos.

Hines M, Carnevale N (1997) The NEURON simulation environment. Neural Computation 9: 1179–1209.

Hodgkin AL, Huxley AF (1952) A quantitative description of membrane current and its application to conduction and excitation in nerve. Journal of Physiology 117: 500–544.

Lindsay KA, Rosenberg JR, Tucker G (2003). Analytical and numerical construction of equivalent cables. Mathematical Biosciences 184: 137–164.

Oram MW, Wiener MC, Lestienne R, Richmond BJ (1999) Stochastic nature of precisely timed spike patterns in visual system neuronal responses. Journal of Neurophysiology 81: 3021–3033.

Poriazi P, Brannon T, Mel BW (2003) Pyramidal neuron as two-layer neural network. Neuron 37: 989–999.

Rall W (1964) Theoretical significance of dendritic trees and motoneuron input-output relations. In: RF Reiss, ed. Neural Theory and Modelling. Stanford University Press, Stanford CA.

Segev I, Burke RE (1998) Compartmental models of complex neurons. In: C Koch and I Segev eds. Methods in Neuronal Modeling—from Ions to Networks, 2nd ed. MIT Press, MA, Ch. 3, pp. 93–136.